Magnetic Resonance Materials in Physics, Biology and Medicine (2022) 35:903–909
https://doi.org/10.1007/s10334-022-01018-2

RESEARCH ARTICLE

High-permittivity pads to enhance SNR and transmit efficiency in MRI of the heart at 7T: a simulation study

Giuseppe Carluccio[1] · **Christopher M. Collins**[1]

Received: 19 October 2021 / Revised: 20 April 2022 / Accepted: 25 April 2022 / Published online: 31 May 2022

Abstract

Objective High-permittivity pads have shown promising results in enhancing SNR and transmit efficiency when used for MRI of the brain, but fewer studies have been conducted to examine the performance of high-permittivity pads in other parts of the patient. In this work, we evaluate the impact on SNR and transmit efficiency distributions when high-permittivity pads with different thickness are positioned near the chest of the patient in combination with a transmit/receive array coil.

Methods The performance of the pads is evaluated through numerical simulations, and both the SNR distribution and the transmit efficiency maps are compared with those obtained when the pads are not present and the distance between the coils and the patient is minimal. The average improvement of SNR and transmit efficiency in the heart is also evaluated for different values of the permittivity of the pads.

Results In the scenario examined, high-permittivity pads can increase SNR and transmit efficiency in the heart volume by as much as 16% and 65%, respectively.

Keywords MRI · High-permittivity · Thorax · SNR · Transmit efficiency

Introduction

Use of High-Permittivity Materials (HPM) in MRI scans is increasingly common, especially in imaging of the brain at 7T and above. HPM have provided very promising results to shape the radiofrequency magnetic (B_1) field in order to improve homogeneity of the fields, to enhance Signal to Noise Ratio (SNR), and improve transmit efficiency (TxEff) [1–5].

The presence of HPM pads enhances the displacement current of electric fields between the coil and the subject, becoming a significant source of B_1 field. If the ratio of B_1 field in the imaging region to electrical field throughout the subject can be improved, SNR and/or transmit efficiency can be improved. While in many cases, the largest advantages are seen in regions of the subject very near the pads [2], depending on the design criteria, it has also been shown that HPM surrounding the region of interest can also improve SNR and TxEff deep within the subject [2, 4, 6]. Mechanisms proposed to explain effects deeper in tissue include the possibility of displacement currents in the pad acting as larger, distributed coils with deeper effective penetration than the conductive coils [4], an improved matching layer for greater efficiency in producing fields throughout the sample [7], and the HPM facilitating propagation of fields from one coil further around the subject [8].

Such improvements have been observed in simulations and experiments for MRI scanners of different static magnetic (B_0) field strength [1–5]. For example, for a 7T scanner, an HPM helmet with a thickness of 8 mm and a permittivity value $\epsilon_r = 115$ was recently designed to improve SNR and transmit efficiency [4] when operating with a transmit and receive coil array, and in experiments, it was observed an SNR improvement in the cerebrum of approximately 21%, and the transmit efficiency enhanced of approximately 56% at the center of the brain, where it is difficult to improve SNR by other means, such as by increasing the number of receive coils [9]. In addition, it was shown both in simulations and experiments that at 3T transmit efficiency can be increased by more than 30% and B_1^+ homogeneity improved when HPM pads are used in the torso [1, 10].

Based on the results of helmets simulations with different values of permittivity, it was possible to determine a

✉ Giuseppe Carluccio
Giuseppe.carluccio@nyulangone.org

[1] New York University School of Medicine, 660 First Avenue, New York, NY 10016, USA

mathematical relationship between field strength and the optimum permittivity value of a HPM helmet with a given shape and thickness [11]. Since the HPM pads impact how the radiofrequency electromagnetic fields propagate, the optimum value of permittivity is affected not only by the operating frequency of the scanner but also by many other factors such as the distance between the coil and the HPM pads, the distance between the pads and the subject, the shape and the dielectric properties of the subject's tissues. Therefore, similar to coil design, every application of HPM may require a specific design and optimization process to provide the best signal in the region of interest.

Most applications of HPM have been focused on the brain, while a significantly smaller number of studies have been done for HPM used for other parts of the human body, such as the torso. In this work, we use numerical simulations to investigate how HPM pads can impact the SNR and transmit efficiency generated by a transmit and receive array coil in the chest, considering both permittivity and thickness of the pads and, therefore, also the distance between the coil and the subject. This work is an extended version of a previously presented conference abstract [12], with considerations on how the presence of the HPM pads affect the SAR distribution.

Methods

The performance of SNR and transmit efficiency when HPM pads are used near the chest is evaluated with numerical simulations and compared to the case when no HPM pad is used and the coils are positioned adjacent to the chest.

A human body model representing an average adult male, "Duke" of the Virtual Family v1.0 [13] at 5 mm isotropic resolution, was imported to commercial FDTD simulation software (xFDTD v6.5; Remcom, inc.). The excitation fields were generated with an 8-channel array of 16 cm-long stripline elements, and in reception, from 24 additional receive-only rectangular loops (each 6 cm wide and 12 cm long) all operating at 300 MHz [14]. The coils were split equally into a "clamshell" configuration with half on either side of the torso (Fig. 1). HPM pads were designed to have a shape conformal to the coil and were positioned between the coils and the body (Fig. 1). HPM pads with different thickness, 1.5 cm and 3 cm, respectively, were tested for several permittivity values, and two optimum permittivity values that provide the highest SNR and transmit efficiency were identified for each pad thickness. For the optimum permittivity value of these two configurations, we have also evaluated the SNR and the transmit efficiency of a transmit array composed of

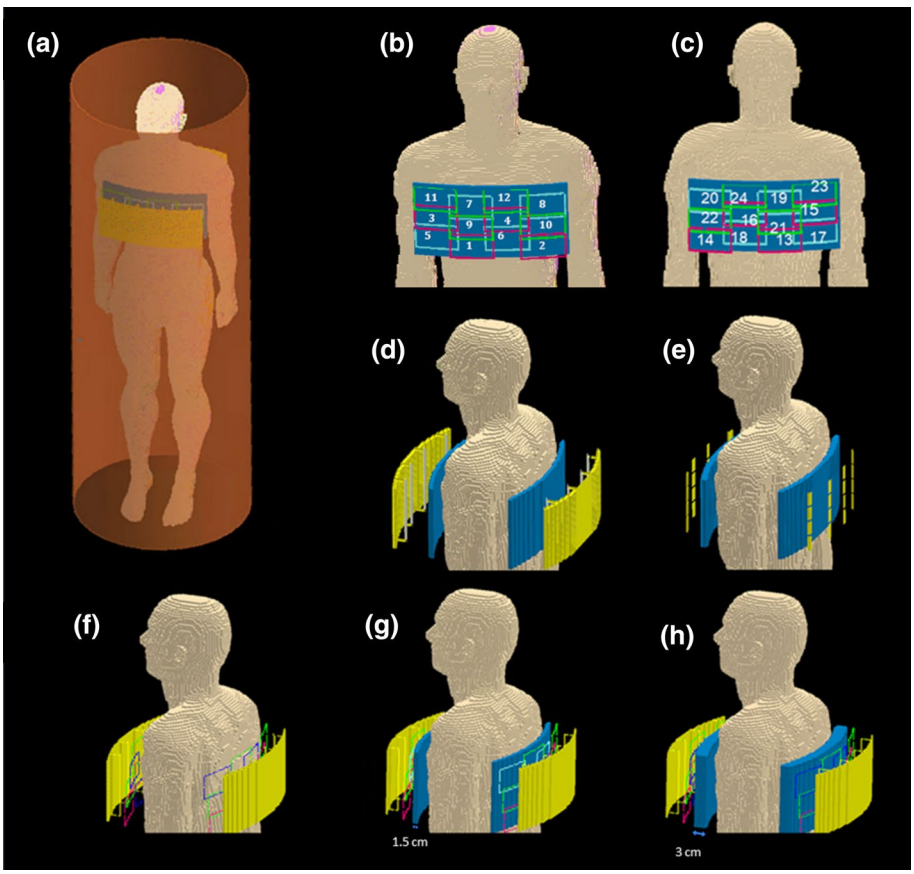

Fig. 1 Geometry of problem. Human body, HPM pads (dark blue), and all coils were simulated in a long magnet bore (**a**). 12 receive coils (red, green, light blue) were simulated on both front (**b**) and back (**c**) of torso. Receive coils were 6 cm high and 12 cm wide (**b**, inset). For transmission, 8 stripline elements (**d**) or 8 dipole antennas (**e**) were used. Cases with no pad and the coils close to the torso (**f**), 1.5 cm-thick pads (**g**), and 3 cm-thick pads (**h**) were simulated. Dimensions for receive coils are given in the inset for **b**, for stripline elements and ground plane are in **d**, for dipoles are in **e**, and for HPM pad thicknesses are in **g** and **h** with other dimensions of the HPM pad matching those of the ground plane in **d**

8 dipoles positioned at the same locations of the striplines (Fig. 1). Both SNR and transmit efficiency were evaluated with in-house Matlab scripts. In addition, the Matlab optimization toolbox has been used to perform an optimization of the homogeneity of the field in the heart for the optimum permittivity values, using as initial values the driving currents that provide the maximum transmit efficiency in the heart. The fields generated by each coil were computed separately. The schematics and the dimensions of the coils are shown in Fig. 2.

The SNR in the location r was computed as

$$\mathrm{SNR}(r) = \sqrt{\Psi(r)^{*} R^{-1} \Psi(r)}, \tag{1}$$

where Ψ is the vector representing the sensitivity of coils in the receive array at the location r [15]. Indicating with N_R the number of receive coils, Ψ has length N_R and each element corresponds to the complex field B_1^- generated at location r by the m^{th} coil,

$$\Psi_m(r) = B^-_{1,m}(r), \tag{2}$$

and R is the noise resistance matrix [16], which has size $N_R \times N_R$. The matrix R was computed by summing the sample matrix R_S (corresponding to the thermal noise from the sample) and the matrix R_C, or coil self-resistance, (which corresponds to the noise in each coil). R_C is a diagonal matrix with each element of the diagonal being the power computed in the corresponding coil. The current is assumed to flow in the cross-section of the coil along the surface in a strip having thickness equal to the skin depth δ [17]. Indicating the width and thickness of the conductor cross-section with w and t, with l the length along its perimeter, each element of the diagonal of R_C is given by,

$$R_{C,m,m} = \frac{\rho l(m)}{2w(m) + 2t(m)\delta}, \tag{3}$$

where ρ is the resistivity of the conductor.

For each couple of coils m and n, the sample matrix R_S is computed by integrating the conjugate product

$$R_{S,m,n} = \int_r \sigma(r) E_m(r) E_n^{*}(r) d^3 r, \tag{4}$$

over all the cells r of the body model. Here, $\sigma(r)$ is the electrical conductivity in the three directions of the cell at the location r, and $E_m(r)$ and $E_n(r)$ denote the electric fields generated at the location r. Being a discretized numerical model, the integral in (4) is computed by summing the conjugate product of the electric fields and local conductivity over all voxels in the body, and the volume $d^3 r$ indicates the volume of a single voxel.

Regarding the transmit field, for each location on two orthogonal planes, one axial plane and a coronal plane near the center of the chest, a maximum achievable local transmit efficiency is calculated using an analytical approach [18]. Assuming weak coupling between the elements of the transmit array, the optimum driving currents for each location is given by

$$I_i(r) = \frac{\left|B^+_{1,i}(r)\right| e^{-j\angle B^+_{1,r}}}{Re\{Z_{ii}\}}, \tag{5}$$

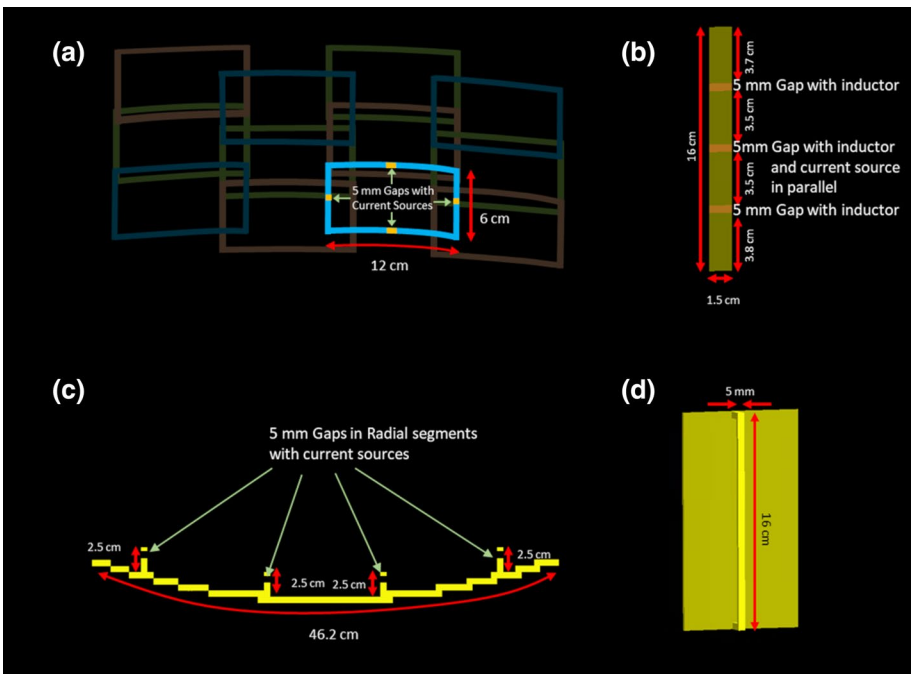

Fig. 2 Geometry of receive coils (**a**), dipole antennas (**b**) and stripline array (**c**, **d**). Receive coils and stripline shield/ground plate are curved as if on an arc with a 53 cm radius. The arc length for the overall receive coil array matches that of the stripline shield/ground plate (46.2 cm). Centers of dipole antennas and stripline elements are spaced as indicated in **c**. The location of the driving components is reported. Inductor values for proper tuning were different for each dipole and configuration, and vary from 84 to 117 nH

where $B^{+}_{1,i}(r)$ is the component of the i^{th} element of the transmit array in the specific location of interest r, and $Re\{Z_{ii}\}$ is the real component of the self-impedance of the i^{th} element of the transmit array. With the driving currents calculated with Eq. (5), the transmit efficiency is computed by evaluating the combined transmit field $B^{+}_{1,i}(r)$ normalized by the same amount of absorbed power.

For each optimum permittivity value, the safety of the transmit array is evaluated by comparing the maximum local SAR averaged on any 10 g volume when the array elements are driven to maximize the transmit efficiency in the heart. The SAR is averaged with a previously presented method [19, 20] when combined fields are normalized to produce 1 μT B^{+}_{1} in the heart.

Results

For each case, the ratios of SNR and transmit efficiency to an "original" case with no HPM pads and with the coil arrays adjacent the chest were calculated at each location through a given plane of the body model. Figure 3 shows distribution of both SNR and transmit efficiency, while Fig. 4 shows the ratios for several values of permittivity of the HPM pad for the two pads with different thickness and for different values of permittivity. The transmit efficiency maps are reported for both the case when striplines and dipoles are used as a transmit array. For a pad thickness of 3 cm we computed SNR up to a permittivity of 125, above which we observed a significant degradation of the SNR in deeper tissues. For a pad thickness of 1.5 cm, we similarly observed an SNR reduction for permittivity values higher than 150. Figure 4 also shows the ratio of SNR when an HPM pad is used to the case when no pad is present and the distance between the coils and the tissues is minimal. In the heart, a maximum

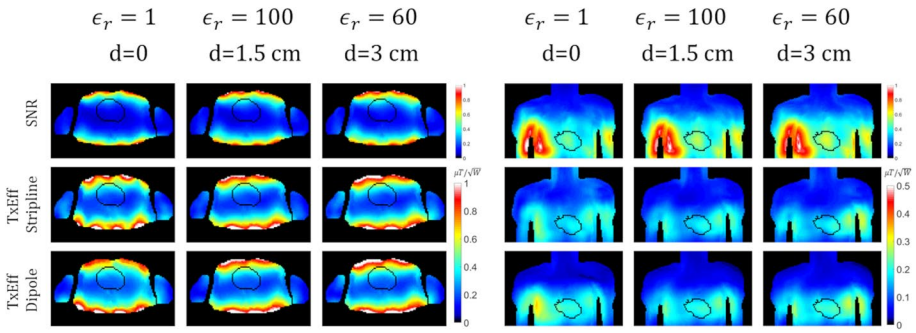

Fig. 3 For axial (first three columns) and coronal (last three columns) views, plots of the SNR (first row) and transmit efficiency for stripline (second row) and dipole array (third row), for the case with no pad on the left, the case with a 1.5 cm HPM pad in the middle, and the case with a 3 cm pad on the right. The SNR figures are normalized to the maximum value of the respective case in the corresponding plane with no pad, such that the axial and coronal views have different normalization factors: the normalization factor for the axial view is 5.4 times larger than the factor for the coronal view For transmit efficiency the scale of the colorbar ranges from 0 to 1 $\mu T/\sqrt{W}$ for the axial view, and 0 to 0.5 $\mu T/\sqrt{W}$ for the coronal view

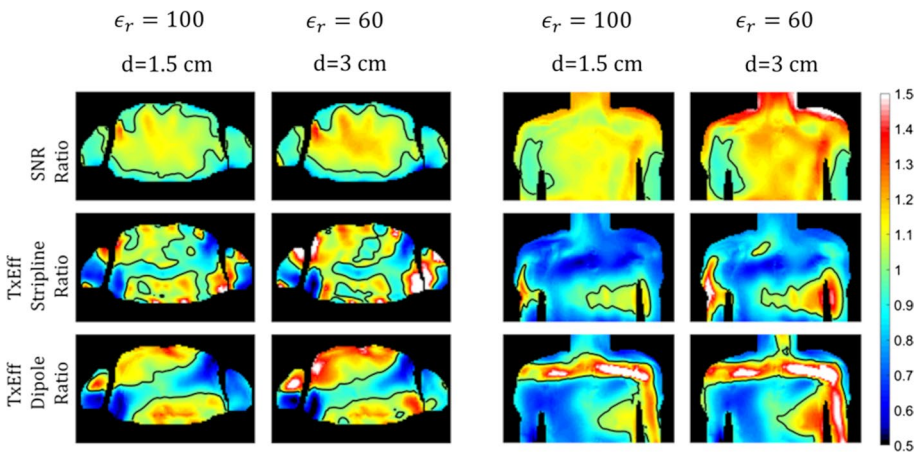

Fig. 4 For axial (first two columns) and coronal (last two columns) views, plots of the voxel-by-voxel ratio of SNR (first row) and transmit efficiency for stripline (second row) and dipole array (third row) to the cases with no pad. The black line corresponds to a ratio of 1

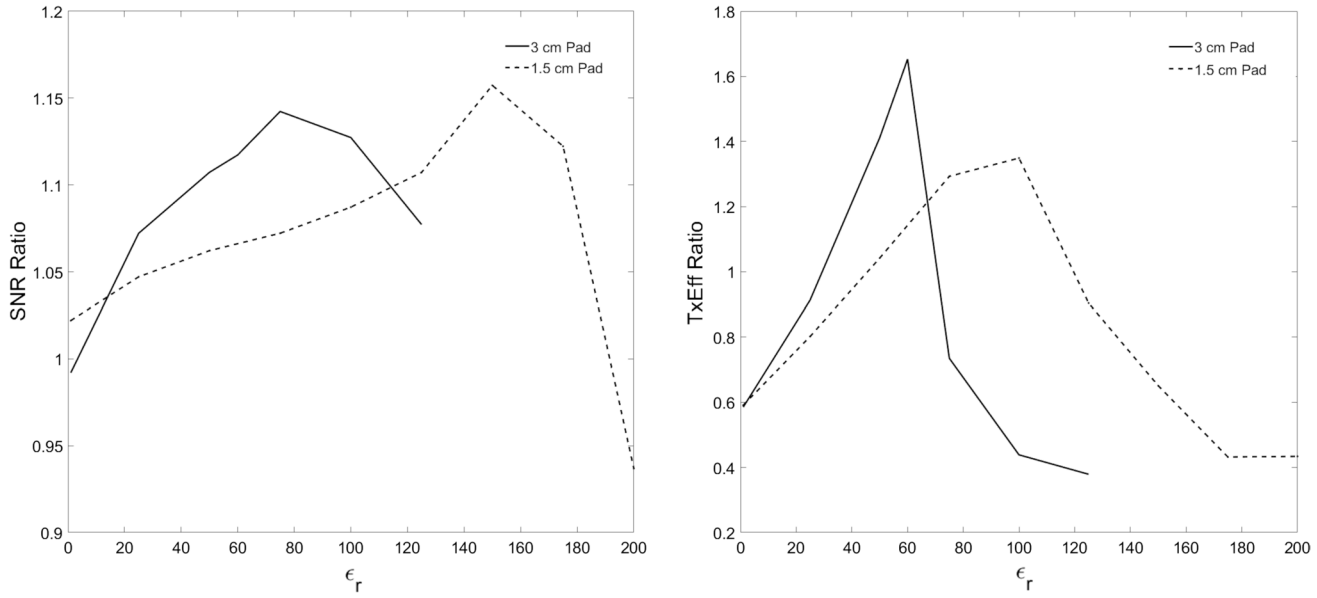

Fig. 5 Ratio of SNR (left) and transmit efficiency (right) to values for baseline case averaged over the heart as functions of permittivity in the 3 cm-thick pad (solid line) and 1.5 cm-thick pad (dashed line)

Table 1 For the receive arrays, increase of the average SNR values in the heart with respect to the case with no HPM pad

Receive array position, permittivity	SNR improvement
$d=0$	0.00%
$d=1.5$ cm, $\varepsilon_r=100$	8.53%
$d=3$ cm, $\varepsilon_r=60$	11.85%

Table 2 For both the two transmit arrays (striplines and dipoles), average transmit efficiency and maximum 10gSAR when the coils are driven to provide the maximum transmit efficiency in the heart

	Transmit efficiency $[\mu T/\sqrt{W}]$	Maximum SAR10g $[W/\text{kg}]$
Stripline ($d=0$)	0.115	35.82
Stripline ($d=1.5$ cm, $\varepsilon_r=100$)	0.123	32.14
Stripline ($d=3$ cm, $\varepsilon_r=60$)	0.129	48.19
Dipole ($d=0$)	0.130	40.54
Dipole ($d=1.5$ cm, $\varepsilon_r=100$)	0.132	27.67
Dipole ($d=3$ cm, $\varepsilon_r=60$)	0.139	45.52

SNR improvement of 16% is observed for a permittivity value of 150 for the 1.5 cm pad.

For the same values of permittivity of the pads, the transmit efficiency distributions were computed, and the ratios of the efficiencies are reported in Fig. 4. The maximum improvement in transmit efficiency in the heart is significant, exceeding 60% for a permittivity value of 60.

The ratios of both the SNR and the transmit efficiencies in the heart with respect to the case with no pad when different permittivity values of the HPM pad are plotted in Fig. 5, while average SNR values in the heart, and transmit efficiency and maximum average 10 g SAR (SAR10g) are reported in Tables 1 and 2. For the thicker pad, the optimal permittivity has a lower value.

A comparison of the power dissipated in the coils, in the HPM pad when the electrical conductivity is set equal to that of distilled water (0.025 S/m), in the tissues, and of the radiated power is reported in Table 3.

The transmit efficiency in the whole heart volume provided by the dipoles is about 10% higher than that provided by the striplines. This is consistent with the values of absorbed power in the tissues reported in Table 3. When pads are present and fields are shimmed for maximum Tx Eff, the dipole array also produces lower maximum local SAR than the stripline array, though it produces greater local SAR when no pad is present. When shimming for maximum homogeneity in the heart, the dipole array consistently produced greater local SAR than the stripline array.

When algorithms to optimize the homogeneity of the field in the heart are used, the dipoles can provide a better homogeneity, with about half the variance. A higher homogeneity (about 60% reduction in variance) is observed when HPM are used for both the striplines and the dipoles.

Table 3 For both the two transmit arrays (striplines and dipoles), comparisons of the dissipated power in the coils, in the pads, in the body model, and the radiated power

	Power in the coil [*W*]	Power in the HPM [*W*]	Power in the tissues [*W*]	Radiated power [*W*]
Stripline ($d=0$)	0.01%	0.00%	95.38%	4.61%
Stripline ($d=1.5$ cm, $\varepsilon_r=100$)	0.00%	6.24%	93.08%	0.68%
Stripline ($d=3$ cm, $\varepsilon_r=60$)	0.02%	10.08%	76.62%	13.28%
Dipole ($d=0$)	0.00%	0.00%	98.78%	1.22%
Dipole ($d=1.5$ cm, $\varepsilon_r=100$)	0.00%	6.12%	93.62%	0.25%
Dipole ($d=3$ cm, $\varepsilon_r=60$)	0.00%	12.61%	87.05%	0.34%

Discussion

We have compared HPM pad designs to work with a transmit and receive array coil for a 7T MRI system to provide signal for the chest. The analysis of the impact of the HPM pads has been performed through numerical simulations. Our simulations show that HPM pads can improve the SNR and the transmit efficiency in the subject's chest. In particular, we found that the best performance is obtained for a relative permittivity of 60 for the 3 cm pads and a relative permittivity of 100 for the 1.5 cm pads. This demonstrates that the design of HPM pads, including the selection of the permittivity, is strictly linked to the geometry of the pads for a specific frequency.

Change in permittivity of the HPM pads affects the SNR distribution, while lower permittivity values provide a more uniform improvement, above a certain point, further increases in permittivity tend to provide stronger improvements only near the surface of the body. According to our simulations, optimal values of permittivity can provide improvements in both the SNR and the transmit efficiency in deep tissues such as in the heart. However, the improvements are not homogeneously distributed in the volume.

The results do not seem to be significantly affected by the distance between the coils and the tissues. In fact, a comparison of the results for the cases without the pad in the two extreme distances (maximum and minimum distance) shows relatively minor differences. The closer coils provide stronger SNR at the surface, while higher SNR can be observed in deeper tissues when the coils are not placed next to the body.

We could observe weak coupling between the elements of the transmit arrays (both the stripline and the dipole arrays), with a maximum value of − 20 dB among the elements and minimal effects of the HPM pads. In contrast, very strong coupling was observed between some loops of the receive array, with a maximum value of − 4.4 dB. However, no decoupling techniques were used to reduce the coupling among the receive coils, and receive coil fields were computed independently with the expectation that in experiment preamplifier decoupling and careful coil overlap would be effective. In addition, we could observe a small increase in the average coupling of the receive array elements when the HPM pads are present, but the maximum coupling values were reached when no pads were present.

While HPM pads can improve coil performance, another consideration is the added weight to the coils, which can affect both ease of use for the MRI technologist, and patient comfort. Water-based HPM pads with the volumes simulated here would weigh approximately 1.12 kg for each 1.5 cm pad and 2.25 kg for each 3 cm pad. Considering the relative weight of coil construction materials, this might easily double the weight of a lightweight coil designed to rest on the chest of the subject.

Use of these pads did not show significant effects on the maximum local SAR when the currents of the transmit array are driven to maximize the transmit efficiency in the heart. When the elements are driven to provide an average total value of B_1^+ in the heart equal to 1 μT, we found maximum 10gSAR values for the case with no pad (35.8 W/Kg and 40.5 W/kg for the stripline and dipole arrays, respectively), slightly lower SAR values for the 1.5 cm thick pad (32.1 W/Kg and 27.7 W/kg), and slightly higher SAR values for the 3 cm pad (48.2 W/Kg and 45.5 W/kg).

In conclusion, we found that HPM pads can be used to enhance SNR and transmit efficiency in the chest without increased risks related to RF safety. SNR increase can be mainly found in deeper tissues, while the vicinity of the coil without the pad provides better performance towards the surface of the body.

Funding This research work was supported by National Institutes of Health, grant numbers: R01 EB0021277, P41 EB017183.

Declarations

Conflict of interest The authors declare that they have no conflict of interest.

Ethical standard This article does not contain any studies involving human subjects.

References

1. Yang QX et al (2013) Radiofrequency field enhancement with high dielectric constant (HDC) pads in a receive array coil at 3.0T. J Magn Reson Imaging 38(2):435–440
2. Brink WM, Webb AG (2014) High permittivity pads reduce specific absorption rate, improve B1 homogeneity, and increase contrast-to-noise ratio for functional cardiac MRI at 3 T. Magn Reson Med 71(4):1632–1640
3. Zivkovic I, Teeuwisse W, Slobozhanyuk A, Nenasheva E, Webb A (2019) High permittivity ceramics improve the transmit field and receive efficiency of a commercial extremity coil at 1.5 Tesla. J Magn Reson 299:59–65
4. Lakshmanan K, Carluccio G, Walczyk J, Brown R, Rupprecht S, Yang QX, Lanagan MT, Collins CM (2021) Improved whole-brain SNR with an integrated high-permittivity material in a head array at 7T. Magn Reson Med 86(8):1167–1174
5. Luo W, Lanagan MT, Sica CT, Ryu Y, Oh S, Ketterman M, Yang QX, Collins CM (2013) Permittivity and performance of dielectric pads with sintered ceramic beads in MRI: early experiments and simulations at 3T. Magn Reson Med 70(1):269–275
6. Carluccio G, Kittivittayakul S, Uslenghi P, Collins CM, Erricolo D (2014) Fast method to compute the electromagnetic field inside a model of the human head surrounded by a dielectric pad. In: ISMRM Annual Meeting in Milan, Italy
7. Carluccio G, Oh S, Yang QX, Erricolo D, Luo W, Collins CM (2013) Near-field wave impedance matching with high-permittivity dielectric materials for optimum transmittance in MRI systems. In: ISMRM Annual Meeting in Salt Lake City, USA
8. Carluccio G, Yang QX, Collins CM (2020) Distribution and propagation of fields and displacement currents in a high-permittivity helmet. In: ISMRM Annual Meeting in Sydney
9. Lattanzi R, Wiggins GC, Zhang B, Duan Q, Brown R, Sodickson DK (2018) Approaching ultimate intrinsic signal-to-noise ratio with loop and dipole antennas. Magn Reson Med 79(3):1789–1803
10. De Heer P, Brink WM, Kooij BJ, Webb AG (2012) Increasing signal homogeneity and image quality in abdominal imaging at 3T with very high permittivity materials. Magn Reson Med 68(4):1317–1324
11. Collins CM Collins CM, Carluccio G, Zhang B, Adriany G, Ugurbil K, Lattanzi R (2019) On the relationship between field strength and permittivity for desired effects of high-permittivity materials in MRI. In: Proceedings of the 25th scientific meeting, International Society for Magnetic Imaging Imaging, Montreal, p 1566.
12. Carluccio G, Collins CM (2021) Use of high—permittivity pads to enhance SNR and transmit efficiency in the chest at 7T. In: Proceedings of the 27th scientific meeting, International Society for Magnetic Resonance Imaging, Vancouver, p. 1396.
13. Christ A et al (2009) The virtual family—development of surface-based anatomical models of two adults and two children for dosimetric simulations. Phys Med Biol 55(2):N23
14. Metzger GJ et al (2010) Performance of external and internal coil configurations for prostate investigations at 7T. Magn Reson Med 64(6):1625–1639
15. Pruessmann KP, Weiger M, Scheidegger MB, Boesiger P (1999) SENSE: sensitivity encoding for fast MRI. Magn Reson Med 42(5):952–962
16. Roemer PB, Edelstein WA, Hayes CE, Souza SP, Mueller OM (1990) The NMR phased array. Magn Reson Med 16(2):192–225
17. Carluccio G, Collins CM (2018) A tool for coil sensitivity analysis for an arbitrary surface coil near arbitrary spherical sample. In: Proceedings of the International Conference on Electromagnetics in Advanced Applications, Cartagena, pp. 521–523.
18. Carluccio G, Collins CM, Erricolo D (2014) A fast, analytically based method to optimize local transmit efficiency for a transmit array. Magn Reson Med 71(1):432–439
19. Catarinucci L, Tarricone L (2012) New algorithms for the specific absorption rate numerical evaluation based on spherical averaging volumes. Prog Electromagnet Res B 44:427–445
20. Carluccio G, Erricolo D, Oh S, Collins CM (2013) An approach to rapid calculation of temperature change in tissue using spatial filters to approximate effects of thermal conduction. IEEE Trans Biomed Eng 60(6):1735–1741